Durability of Glass Polymer Composites Subject to Stress Corrosion

Amar Khennane[1] and Robert E. Melchers, F.ASCE[2]

Abstract: Although it is well known that moisture ingress in glass fiber reinforced polymers (GFRP) enhances the phenomenon of stress corrosion cracking in the fibers, and that this reaction is likely to proceed more rapidly at the weakest sites in the glass fiber surface, a fundamental law that would permit the valid extrapolation of stress rupture curves to long service lives is yet to be developed. As a result, design guidelines for glass fiber reinforced polymers components have been developed mainly on a prescriptive rather than of a performance basis. Based on the well established knowledge on the chemical behavior of glass and, in particular, that of glass flaws, a model that combines fracture mechanics, shear lag theory, and a probability model for flaw size is developed to describe the behavior of GFRP composites. The predicted results, although limited to rather idealized situations, are very encouraging. They suggest that, with only modest assumptions about material properties, it is possible to obtain mechanisms of GFRP breakdown, which correspond with observed experimental behavior.

DOI: 10.1061/(ASCE)1090-0268(2003)7:2(109)

CE Database subject headings: Durability; Fiber reinforced polymers; Fiberglass; Corrosion; Cracking.

Introduction

Moisture induced stress–strain corrosion in glass reinforced plastics is increasingly being seen as a critical issue for the introduction of composite technology to applications where long term durability is important, such as for civil engineering applications. For these, structural components must be able to demonstrate satisfactory performance, with 50 or 100 years lifetime being typical requirements. And in some applications, they must also do so at stress levels that are significant fractions of their ultimate strengths, and often in aggressive environments. The issue of long-term durability is critical as little published long-term data exist for resins and composites, and glass fiber is known to be highly sensitive to moisture, salt, acidic and alkaline solutions, and stress corrosion/creep rupture. As a result, design guidelines for glass fiber reinforced polymer (GFRP) components have been developed mainly on a prescriptive rather than on a performance basis. Roberts (1978), cited in Lyons and Phillips (1981), described three bases used to determine the design stress for such components. The first consists of using the tensile strength obtained from a short-term test, and then dividing it by a ''factor of safety,'' usually in the range of 8–16. The second approach is to specify a permissible design strain and to multiply it by the short-term modulus of elasticity. As a third approach, long-term stress–rupture tests could be performed, and the design stress could be chosen from a given lifetime. The stress levels so obtained would be reduced by a further factor of safety, again arbitrary, to allow for the detrimental effects of the environment. The principal reasons for three approaches, as identified in Roberts (1978) and Lyons and Phillips (1981), is the lack of fundamentals laws, which permit the valid extrapolation of stress–rupture curves to long service lives.

It might be noted that there is a worldwide trend for building design codes and similar infrastructure design guides to be revised from a prescriptive to a performance basis. To achieve consistency and transparency of the requirements across all relevant structural materials, composites structures would be expected to be consistent also. Given the fact that the use of composites in the infrastructure industry is relatively recent, and that there is a lack of an ''experience of use'' basis, the development of performance criteria demonstrating compliance with such criteria is an apparent need. To meet this need and, therefore, contribute to the wider acceptance of composites by the infrastructure industry, it is considered that analytical methods that help explain and promote an understanding of the mechanisms and rates of environmental degradations for GFRP are required. The aim of this paper is to present an analytical approach based on micromechanics modeling of the phenomenon of environmental stress corrosion in GFRP.

In the next section, an overview of the chemical aspects of stress corrosion in glass is presented. The ''Role of Flaws and their Characterization'' section deals with the nature of flaws in glass fibres and their characterization. The theory behind the model to describe the stress corrosion rate in a glass fibre is presented in ''Modeling of Stress Corrosion Cracking of a Glass Fiber.'' This is followed by ''Stress Corrosion of a Glass Fiber Reinforced Polymer,'' where the model for the stress corrosion of a fibre is implemented within the framework of the shear lag theory to describe the mechanism of failure of GFRP. Finally, a summary of the concluding remarks is presented in the ''Conclusion.''

[1]Lecturer, Faculty of Engineering and Surveying, Univ. of Southern Queensland, Qld 4350, Australia; formerly, Research Associate, Dept. of Civil, Surveying, and Environmental Engineering. The Univ. of Newcastle, NSW 2308, Australia. E-mail: Khennane@usq.edu.au

[2]Professor, Dept. of Civil, Surveying, and Environmental Engineering, The Univ. of Newcastle, NSW 2308, Australia.

Note. Discussion open until October 1, 2003. Separate discussions must be submitted for individual papers. To extend the closing date by one month, a written request must be filed with the ASCE Managing Editor. The manuscript for this paper was submitted for review and possible publication on August 14, 2001; approved on February 13, 2002. This paper is part of the ***Journal of Composites for Construction***, Vol. 7, No. 2, May 1, 2003. ©ASCE, ISSN 1090-0268/2003/2-109–117/$18.00.

Environmental Stress Corrosion in Glass Fiber Reinforced Polymer

The stress corrosion of glass was studied as early as the late fifties by Charles (1958a,b). Since then, it has been established (Mould 1960; Wierderhorn and Bolz 1970) that the failure of glass is governed by surface flaws, which concentrate applied stresses to critical values. One view is that stress plays a role similar to that of temperature in expanding the structure of the glass and easing the freeing of Na^+ ions from tight interstices. According to Charles (1958a,b) who postulated a corrosion mechanism for glass, only the terminal end, which associates Na^+ ion to the glass network, is responsible for dissolution. This initial dissolution happens according to Eq. (1)

$$\left[\begin{array}{c} | \\ -Si-O-Na \\ | \end{array}\right] + H_2O \rightarrow - \begin{array}{c} | \\ SiOH \\ | \end{array} + Na^+ + OH^- \qquad (1)$$

An oxygen sodium bond near the interface is broken by the migration away of a Na^+ ion and the oxygen atom dissociates a water molecule to satisfy its force field with a hydrogen ion. Free hydroxyl ion is formed in the process and enables the second reaction, Eq. (2), to take place

$$\left[\begin{array}{ccc} | & & | \\ -Si-O- & & Si- \\ | & & | \end{array}\right] + OH^- \rightarrow - \begin{array}{c} | \\ Si-O-H \\ | \end{array} + - \begin{array}{c} | \\ SiO^- \\ | \end{array} \qquad (2)$$

In step (2), which cannot take place if step (1) has not happened, the very strong Si—O—Si bond is broken. One end of the break becomes a silanol end by hydroxyl ion attachment and the other produces an end structure capable of dissociating another water molecule according to Eq. (3)

$$\left[\begin{array}{c} | \\ -SiO^- \\ | \end{array}\right] + H_2O \rightarrow - \begin{array}{c} | \\ SiOH \\ | \end{array} + OH^- \qquad (3)$$

This step is essentially the same as the first, but it could not occur unless steps (1) and (2) preceded it. One might be tempted to bypass step (1) by writing

$$\left[\begin{array}{ccc} | & & | \\ -Si-O- & & Si- \\ | & & | \end{array}\right] + H_2O \rightarrow 2\left[\begin{array}{c} | \\ -Si-O-H \\ | \end{array}\right] \qquad (4)$$

According to Charles (1958a,b), this reaction has little significance in glass dissolution. He argued that at moderate temperatures (100°C–300°C) and in the presence of water vapor, fused silica remains essentially unaltered for long periods of time whereas a glass containing alkali structures as well as the unending silica network, quickly undergoes severe decomposition. This also explains why quartz or fused quartz is insoluble in water at a neutral pH and moderate temperatures.

The action of water on glass is one of diffusion and disintegration. Water chemically reacts with the components of the glass, and this reaction is likely to proceed more rapidly at the weakest sites in the glass surface, namely structural flaws, resulting in crack surface corrosion. The corroded material generally loses its coherency and decrepitates by exfoliation of layers or by a blockwise disintegration (Charles 1958a,b).

As in bulk glass, the premise for stress corrosion in glass fibers is that a stress corrosion crack initiates at a pre-existing flaw in a glass fiber. The crack then grows under stress and finally leads to breakage of the fiber. However, in GFRP this can happen only after aggressive environment components have diffused through the resin protecting the glass fibers. This is the phenomenon of environmental stress corrosion and for glass fibers, including those embedded in a polymer matrix, has been studied by many researchers. An excellent review of the subject is given in Schutte (1994). For aqueous environments, more details are given in (Schmitz and Metcalfe 1966; Lyons and Phillips 1981; Hogg and Hull 1982; Phillips 1983). For dilute acids, reference might be made to (Hogg and Hull 1982; Aveston and Sillwood 1982; Lhymn and Schultz 1983; Hsu et al. 1986; Price and Hull 1987).

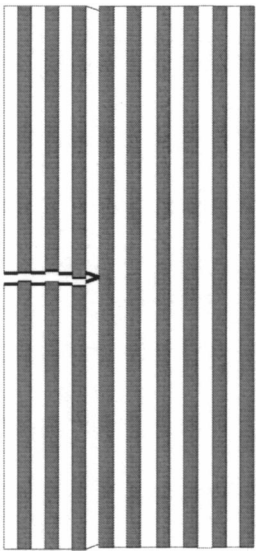

Fig. 1. Fracture processes occurring in glass fiber reinforced polymer tested in corrosive environment

Glass is also subject to stress corrosion cracking in acidic environments at a much accelerated rate. Price and Hull (1987) reported that spontaneous fracture of glass fibers was found to occur when the fibers were subjected to mineral acids with and without applied stress. The chemical aspect of glass stress corrosion in acidic environments is different from that in aqueous environments. It is due largely to an ion exchange between metallic cations in the fibers and the hydrogen ions in the acid resulting in direct leaching of the glass surfaces.

Hogg and Hull (1982) described the main phenomenological characteristics of stress corrosion of glass reinforced composites. A very important feature is the planar nature of the fracture surfaces. In contrast to fracture in the absence of a corrosive environment, the initial fracture surface is planar with only a small amount of fiber pullout, as shown in Fig. 1. The fracture surface of each fiber is usually characterized by a very smooth, mirrorlike zone surrounded by a hackle zone. The mirror zone is due to stress corrosion and the hackle zones are due to brittle fracture. This failure is always associated with tensile strains and does not occur in regions of compressive strain. The time to failure depends on the environment type and is closely related to its interaction with the glass fibers.

Role of Flaws and Their Characterization

From the aforementioned description, it is evident that stress corrosion failure of GFRP is closely linked to the flaws in the fibers. These flaws act as stress risers. Their presence promotes stress corrosion cracking in the fiber. The matrix material serves mainly

J. Compos. Constr. 2003.7:109-117.

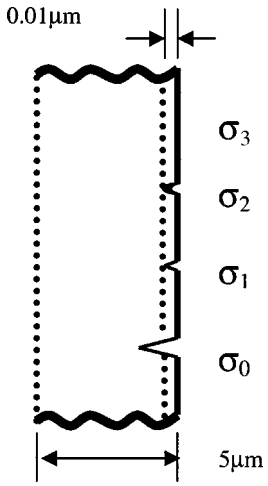

Fig. 2. Schematic representation of flaws on surface of glass fiber (Bartenev 1969)

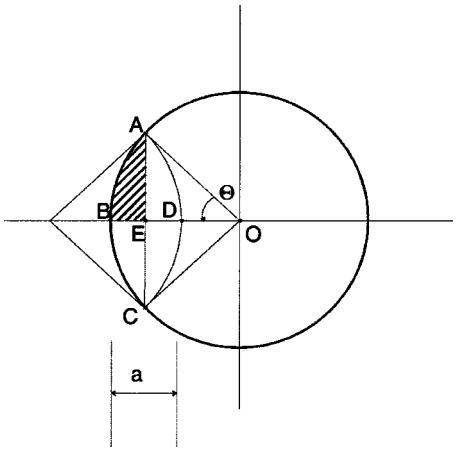

Fig. 3. Shape of stress corrosion crack in crack fiber (Sekine and Beaumont 1998)

to transfer the load between the fibers. This is governed by matrix material elasticity and debonding with sliding friction between the fiber and matrix. The two factors controlling fiber failure are (1) the statistical distribution of fiber flaws, and (2) the stress distribution along the fiber direction. For bulk glass, structural flaws have been estimated to be elliptical in shape and about 5 μm long. But, since fibers might have an average diameter of only about 9 μm, a surface fault of this magnitude would have catastrophic effects (Loewenstein 1973).

According to Schmitz and Metcalfe (1965) flaws in glass fibers are extremely small. Conventional methods of examination are difficult to use and even if successful, the results do not readily describe the effect of the flaws on strength. As a result, an indirect method has been used to characterize the flaws. It consists of a logarithmic plot of fiber strength versus sample length. Typically, the plot is linear, but only for limited ranges of gauge lengths (lengths of the fiber sample tested). The explanation, which has been offered for such a result is that two distributions of flaws are present on the fibers. One distribution of flaws controls failure for long lengths (type A) and other one (type B) controls failure for short lengths. Type A flaws are 2 cm apart on the average and are believed to be deep pits or scratches. Type B flaws have an average separation of 10^{-2} cm or less and are believed to be shallow etch pits formed by water vapor attack.

Combining the technique of UV light absorption and hydrofluoric acid etching, Bartenev (1969) also characterized the different types of flaws in a glass fiber. According to his representation, shown in Fig. 2, three levels of strength, σ_0, σ_1, and σ_2, correspond to three different types of flaws present on the surface of a glass fiber. The level of strength σ_0 was found to result from heat treatment, which leads to microcracks having a depth comparable to half the radius. The strength level σ_1 corresponds to surface submicrocracks generated during the drawing of the fiber. In general, their depth is less than the surface layer of 0.01 μm. Strength level σ_2 corresponds to the existence of microruptures on the surface of the fiber, these also occur during drawing. The stress level σ_3 corresponds to the strength of flawless glass. Even though the description given in (Bartenev 1969) is more precise in terms of the size and shapes of the individual flaws, it does not consider the distribution of the different flaws over the fiber length. Comparing the two flaw characterizations just described, it is possible that type A and type B flaws of Schmitz and Metcalfe (1965) correspond, respectively, to the σ_1, σ_2 flaws of Bartenev (1969). Using the descriptions given herein, the following section attempts to demonstrate that this equivalence is likely.

Modeling of Stress Corrosion Cracking of Glass Fiber

Sekine et al. (1998) Model for Stress Corrosion Cracking of Glass Fiber

Based on the equation for the rate of stress corrosion of bulk glass in water (Wierderhorn and Bolz 1970), given as

$$\frac{da}{dt} = \nu \exp\left(-\frac{E_a - \alpha K_I}{RT}\right) \tag{5}$$

where a = length of the crack; E_a = activation energy; K_I = stress intensity factor for opening mode; R = gas constant; T = absolute temperature; and ν and α = empirical constants. Sekine et al. (1991, 1995, 1998) developed a theory to study the stress corrosion cracking of a glass in acid. Eq. (5) was rewritten such that it takes into account the concentration of acid

$$\frac{da}{dt} = nk_{s0}C_E \exp\left(\frac{\alpha K_I}{RT}\right) \tag{6}$$

where n = molar ratio of glass to acid; k_{s0} = reaction rate constant of glass to acid; and C_E = the concentration of acid. By assuming that the shape of a flaw in a fiber is circular, as represented in Fig. 3, Sekine et al. (1998) rewrote Eq. (6) in the form of the rate of increase of the half angle θ with time

$$\frac{d\theta}{dt} = \frac{nk_{s0}C_E}{2r\sin\theta} \exp\left(\frac{\alpha K_I}{RT}\right) \tag{7}$$

By further assuming that the stress intensity factor K_I can be approximated as

$$K_I = \sigma\sqrt{1-\cos(\theta)}\sqrt{2\Pi r} \tag{8}$$

Eq. (7) was integrated between θ_0 (initial angle) and θ_F (final angle) to obtain the time t_F it takes to a fiber to rupture by stress corrosion

$$t_F = \frac{4rRT}{nk_{s0}C_E\alpha\sigma\sqrt{\Pi r}}\left(\frac{RT}{2\alpha\sigma\sqrt{\Pi r}} + \frac{\theta_0}{2}\right)e^{-\alpha\sigma\sqrt{\Pi r}/RT\theta_0} \tag{9}$$

J. Compos. Constr. 2003.7:109-117.

Table 1. Data for Rupture Life Predictions of E-glass in Two Different Environments

Acidic environment	Aqueous environment
$nk_{s0}C_E = 2.05\times10^{-15}$ m/s	$E = 1.212\times10^{5}$ J/mol
$Ca = 2.05\times10^{-15}$ m/s	$\ln \nu = 5.5 \Rightarrow \nu = 244.7$
$\alpha = 0.116$ m$^{5/2}$/mol	$Cw = 9.763\times10^{-20}$
$r = 5\times10^{-6}$ m	$\alpha = 0.138$
$T = 296$ K	$r = 5\times10^{-6}$ m
$R = 8.31$ J/mol/K	$T = 296$ K
	$R = 8.31$ J/mol/K

Once the time t_F was found, Sekine et al. (1998) extended the fiber model to approximate the stress corrosion of a laminate. By assuming that the time required to the brittle fracture of a glass fiber and surrounding matrix is much shorter that t_F, they went on to estimate the macroscopic propagation rate in the laminate as being the ratio of the distance between two rows of fibers divided by the time t_F. The distance between two fibers takes different values depending on the disposition of the fibers. However, this approach is not consistent with the random nature of fiber flaws. If such an approach is used, there is the difficulty of choosing the localization of the initiation of the crack. Or in a composite structure, a stress corrosion crack is likely to initiate at the weakest point; that is the point where the fiber with the biggest flaw is localized, which is completely random in nature.

Calibration of the Sekine et al. Fiber Model

When the values of the parameters ν, E_a, α (for water), and n, k_{s0}, C_E (for acid) are known Sekine et al. (1991, 1995), the values θ_0, r, T, and σ are set, and the rupture life of an E-glass fiber can be predicted in the two different environments. For the acid environment, use is made of the data provided in (Sekine et al. 1991, 1995, 1998) obtained in 0.5N HCl. For the aqueous environment, the data given in (Wiederhorn and Bolz 1970) obtained for an aluminosilicate glass tested in water at 25°C are adopted since the composition of this glass is very close to that of E-glass. The values of the different parameters are shown in Table 1.

The results of numerical simulations carried out with the above data are shown in Fig. 4 for water and in Fig. 5 for acid. The stress levels considered range from 0.3 GPa to 3.3 GPa. Since, as discussed previously, the shapes and sizes of the flaws are not exactly known, different values of the initial angle θ_0 were used. It can be seen that each value of θ_0 gives a different curve.

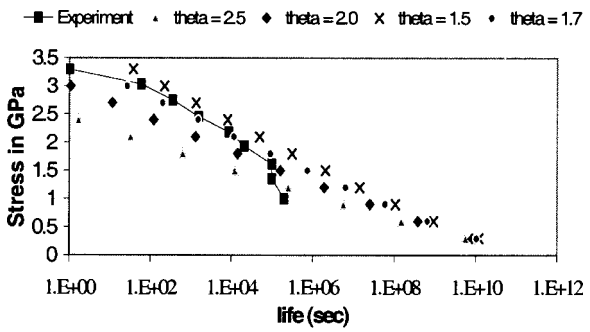

Fig. 4. Simulated stress corrosion of glass fibers in water

In Fig. 4, where the experimental results of Schmitz and Metcalfe (1966) are shown also, it can be seen that the value of $\theta_0 = 1.7°$ corresponds most clearly with the experimental results. In contrast, the value $\theta_0 = 2.5°$ used by Sekine et al. (1998) in their simulation work, and which corresponds to a flaw with a depth of 0.01 μm, does not lead to a particularly good agreement with the experimental results. It underestimates the life of the fibers. Considering that the results reported in (Schmitz and Metcalfe 1966) were obtained for a fiber gauge length of 2.54 cm (1 in.), this suggests that flaw A, which has a lower probability of occurrence over the same gage length than flaw B, corresponds indeed to flaw σ_1 having a typical depth of 0.01 μm.

Fig. 5 shows the simulation results for acid. Unfortunately, there appears to be no experimental evidence available to suggest which value of θ_0 would be most appropriate to provide a better estimate of lifetime. Limited data for short-term exposure does provide an estimate of the ultimate strength. This is best predicted with a half angle $\theta = 1.7°$.

In passing, we note that in comparing Figs. 4 and 5, it appears clearly that the phenomenon of stress corrosion in acids proceeds at a much faster rate than in water as proven by experimental evidence.

Stress Corrosion of Glass Fiber Reinforced Polymer

General

The previous section has shown how the Sekine et al. (1998) model for the stress corrosion failure of a glass fiber can be calibrated against limited experimental results. The present section deals with the stress corrosion of a bundle of fibers embedded in a matrix material. The fibers are assumed to be straight and in tension. However, instead of trying to approximate the macroscopic rate of a stress corrosion crack, which is not consistent with the random nature of fiber flaws, the life of the bundle is obtained here as a sum of the lives of the individual fibers. However, once a fiber breaks a mean of redistributing the stresses to the neighboring unbroken fibers is needed. This can be illustrated in a simple manner through the shear lag theory.

Shear Lag Model

In a real unidirectional composite, the stress in an individual fiber depends on the overall applied stress but also on how the stress is transferred from a broken fiber to the surroundings. As a result,

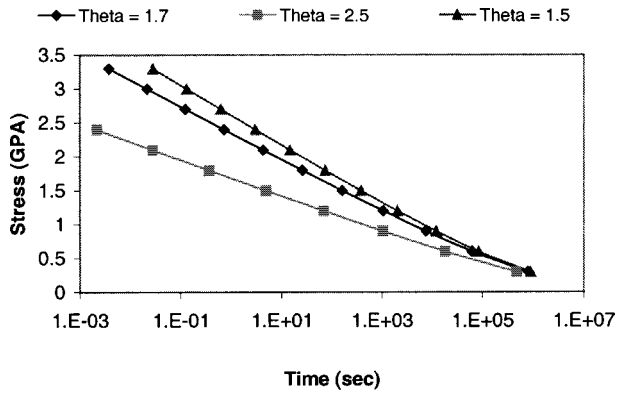

Fig. 5. Simulated stress corrosion of glass fibers in acid

J. Compos. Constr. 2003.7:109-117.

the macroscopic behavior depends very much on the details of the load distribution throughout the composite. This is a complex phenomenon as it depends on the probability of fiber fracture and the sequencing of fiber fracture. Numerical simulation of this phenomenon seems to be an appropriate solution strategy. Therefore, in order to simulate the fracture process of unidirectional GFRP subject to environmental stress corrosion, a mathematical description is needed of the redistribution of stresses in broken fibers to the neighboring unbroken ones. The problem of load transfer from a broken fiber to the surrounding has been studied in the past, and different strategies have been developed. All of this work is concerned with simulation of deterioration of load capacity, not with lifetime prediction.

The earliest study of the stress distribution around broken fibers in a three-dimensional (3D) unidirectional composite with aligned breaks was based on the shear lag theory (Hedgepeth and Van Dyke 1967). Sastry and Phoenix (1993) later improved this to include nonaligned breaks. More recent numerical work, the local load sharing approach analyzed the tensile failure of unidirectional composites (Zhou and Curtin 1995). The finite-element method can also capture many of the key mechanical aspects, however, its use at such a scale is computationally very intensive (Reedy 1984).

For small composites that contain less than 100 fibers, the shear lag approach coupled to a finite-difference scheme (Oh 1979; Goda and Fukunaga 1989; Goda and Phoenix 1994) appears to be a good compromise between quality and computational efficiency. It has been shown (Reedy 1984) that when the matrix behaves elastically, the stress distributions determined with the shear lag model are in good agreement with 3D finite-element analysis.

In the shear lag model, the fibers sustain the axial force, and the matrix transfer through shear the forces lost at broken fibers to the neighboring intact fibers. The model does not take into account the normal stress working in the matrix. The stresses working on the composite are assumed to be therefore those working on the fibers. According to Goda and Phoenix (1994), for polymer composites, the difference is typically small, which justifies the use of this assumption.

The shear lag equations of equilibrium of a circular monolayer, such as the one shown in Fig. 6, are given as follows (Goda and Phoenix 1994)

$$A\frac{d\sigma_1}{dx}+h\tau_1-h\tau_N=0$$

$$\cdot\cdot$$

$$A\frac{d\sigma_i}{dx}+h\tau_i-h\tau_{i-1}=0 \tag{10}$$

$$\cdot\cdot$$

$$A\frac{d\sigma_N}{dx}+h\tau_N-h\tau_{N-1}=0$$

where σ_i $(i=1,N)$ = normal stress working along the ith fiber in the direction x; A = cross-sectional area of the fiber; h = thickness of the monolayer; and τ_i $(i=1,N)$ = shear stress in the matrix between the ith and the $(i+1)$th fiber.

In the present study, each fiber element is assigned a flaw of a half angle θ from a normal distribution. The fibers are assumed to behave in a linear elastic manner. The polymer matrix is assumed to behave according to an elastic perfectly plastic law. Guild et al. (1994) showed that at high strains, the stress transfer from the matrix to the interface is affected by matrix plasticity. This idealized behavior is approximated by the following relationship given in (Goda and Fukunaga 1989) with a hardening parameter $\beta=0.01$

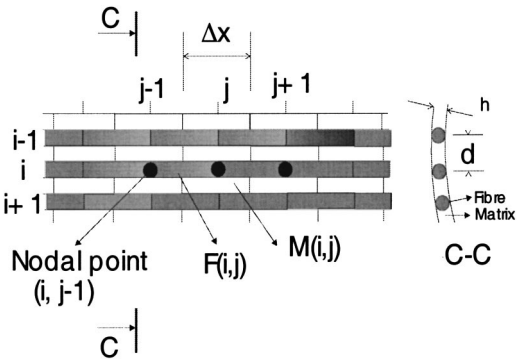

Fig. 6. Finite-difference model used in present simulation (circular monolayer)

$$\tau_i=G(u_{i+1}-u_i)/d_i \quad \text{for } \tau_y>|G(u_{i+1}-u_i)/d_i|$$

$$\tau_i=\beta G(u_{i+1}-u_i)/d_i+(1-\beta)\tau_y \quad \text{for } \tau_Y\leq|G(u_{i+1}-u_i)/d_i| \tag{11}$$

$$\tau_i=0 \quad \text{for } \tau_{\max}\leq|\beta G(u_{i+1}-u_i)/d_i|+(1-\beta)\tau_y$$

where G = elastic shear modulus of the matrix; d_i = distance between the ith and the $(i+1)$th fiber; τ_y = shear yield stress of the matrix; and $\tau_{\max}$ = matrix shear strength. The fiber slip and debonding can also be taken into account through the approach proposed in (Goda and Phoenix 1994). Fiber slip is neglected in the present study since, as was noted earlier, little or no fiber pullout occurs in stress corrosion (see Fig. 1).

Finite-difference Scheme

The simultaneous differential Eq. (10) were solved with the help of the finite-difference method according to a scheme developed by Oh (1979). Fig. 6 shows the discretized model. For simplicity, the fibers are assumed to be uniformly spaced. A fiber element $F(i,j)$ is located between the nodes $(i,j-1)$ and (i,j) and a matrix element $M(i,j)$ is located between the nodal points (i,j) and $(i+1,j)$. In terms of displacements, Eq. (10) can be rewritten as

$$EA\frac{d^2u_i}{d^2x}+\frac{Gh}{d}(u_{i-1}-2u_i+u_{i+1})=0 \quad \text{for } i=1 \text{ to } N \tag{12}$$

where E = Young's modulus of the fiber and d = distance between the fibers.

If the displacement of node (i,j) is approximated by $U_{i,j}$, the second-order term of Eq. (12) can be approximated by

$$\frac{d^2u_{i,j}}{d^2x}=\frac{u_{i,j-1}-2u_{i,j}+u_{i,j+1}}{(\Delta x)^2} \tag{13}$$

where Δx = length of a fiber element.

However, once the fiber element (i,j) breaks, Eq. (13) does not hold. It must be replaced by

$$\frac{d^2u_{i,j}}{d^2x}=\frac{4(u_{i,j+1}-u_{i,j})}{3(\Delta x)^2} \tag{14}$$

The details of this derivation can be found in (Oh 1979; Goda and Phoenix 1994).

J. Compos. Constr. 2003.7:109-117.

By substituting Eqs. (13), (14), and (11) in Eq. (12), the following discrete form of the equilibrium equations can be obtained

$$4EA[\alpha_{i,j}(u_{i,j-1}-u_{i,j})+\alpha_{i,j+1}(u_{i,j+1}-u_{i,j})]/[(2+\alpha_{i,j}+\alpha_{i,j+1})\times(\Delta x)^2]+h[G\beta_{i-1,j}(u_{i+1,j}-u_{i,j})/d+(1-\beta'_{i-1,j})\tau_y \operatorname{sgn}(u_{i-1,j}-u_{i,j})]+h[G\beta_{i,j}(u_{i+1,j}-u_{i,j})/d+(1-\beta'_{i,j})\tau_y \operatorname{sgn}(u_{i+1,j}-u_{i,j})]=0 \quad (15)$$

The terms $\alpha_{i,j}$ = Heaviside's step functions determined by whether the fiber element is broken or not. The constants $\beta_{i,j}$ and $\beta'_{i,j}$ are subject to the state of the matrix element $M(i,j)$ as indicated in Eq. (11). The function sgn(:) is either to -1 or $+1$ depending on whether the sign of the value in brackets is negative or positive. The meanings of the terms $\alpha_{i,j}$, $\beta_{i,j}$, and $\beta'_{i,j}$ are given as

- $\alpha_{i,j}=1$ fiber element $F(i,j)$ not broken;
- $\alpha_{i,j}=0$ fiber element $F(i,j)$ broken;
- $\beta_{i,j}=\beta'_{i,j}=1$ for $\tau_y>|G(u_{i+1}-u_i)/d|$ (elastic behavior);
- $\beta_{i,j}=\beta'_{i,j}=\beta$ for $\tau_y\leqslant|G(u_{i+1}-u_i)/d|$ (plastic behavior); and
- $\beta_{i,j}=0$, $\beta'_{i,j}=1$ for $\tau_{\max}\leqslant|G(u_{i+1}-u_i)/d|+(1-\beta)\tau_y$ [rupture of element $M(i,j)$].

Eq. (15) can be expressed in a more compact form as

$$C_{1(i,j)}u_{i,j-1}+C_{2(i,j)}u_{i-1,j}+C_{3(i,j)}u_{i,j}+C_{4(i,j)}u_{i+1,j}+C_{5(i,j)}u_{i,j+1}=C_{(i,j)} \quad (16)$$

where

$$C_{1(i,j)}=4\alpha_{i,j}/(2+\alpha_{i,j}+\alpha_{i,j+1})$$

$$C_{2(i,j)}=P\beta_{i-1,j}$$

$$C_{3(i,j)}=-4(\alpha_{i,j}+\alpha_{i,j+1})/(2+\alpha_{i,j}+\alpha_{i,j+1})-P(\beta_{i-1,j}+\beta_{i,j})$$

$$C_{4(i,j)}=P\beta_{i,j}$$

$$C_{5(i,j)}=4\alpha_{i,j+1}/(2+\alpha_{i,j}+\alpha_{i,j+1})$$

$$C_{(i,j)}=-dP\tau_y[(1-\beta'_{i-1,j})\operatorname{sgn}(u_{i-1,j}-u_{i,j})+(1-\beta'_{i,j})\operatorname{sgn}(u_{i+1,j}-u_{i,j})]/G$$

where $P=Gh(\Delta x)^2/EAd$.

Introducing the boundary conditions

$$u_{i,0}=0, \quad \text{and} \quad u_{i,k}=\sigma_{ap}\frac{\Delta x}{E}-u_{i,k-1} \quad \text{for} \quad i=1,N$$

Eq. (16) can be rewritten as a set of $N^*(k-1)$ linear equations that can be solved by the elimination method.

Simulation Procedure

The time to failure is computed according to a scheme similar to that developed by McBagonluri (1998). Fig. 7 shows the algorithm of the simulation procedure. In the present case, each fiber element is assigned a half angle θ generated from an appropriate statistical distribution of flaw size. To avoid edge effect, the edge elements are assigned the smallest half angle θ. This ensures that they will be the last elements to fail. Once this is done, the linear system of Eq. (16) is formed and solved to obtain the nodal displacements and the stresses in the elements. Using Eq. (9), the failure time is estimated for each element. The smallest time, Δt, is chosen as the one that will give the next fiber break. A check is then made as to whether the composite has failed or not. If the composite has failed, the process is stopped and its life recorded

BEGIN

STEP 1 *From a normal distribution assign a flaw of a half angle θ to each fibre element*

STEP 2 *Time = 0*

STEP 3 *Give the initial boundary conditions and the initial constants of state*

STEP 4 *Calculate each nodal displacement by solving the set of linear equations and estimate each element stress.*

STEP 5 *Using equation (5), find the smallest time (Δt) that will give the next fibre break. Time = Time + Δt*

STEP 6 *Has the composite failed?*

If **NO** *Update the half angle θ for all the non failed fibre elements due to corrosion that occurred during Δt. For failed fibre elements and matrix elements update the constants of state.* **GOTO STEP 4**

If **YES** *Life = time* **END**

Fig. 7. Algorithm of simulation

as the sum of the individual time elements $t_f=\Sigma\Delta t_i$. If the composite has not failed, the half angle θ must be updated for all the nonbroken elements and since stress corrosion will have occurred during the time Δt,. Since there is no expression that gives the angle θ at the end of an elapsed period of time t_f, this has to be updated by integrating numerically Eq. (7). Once t_F is obtained, it is split into smaller time increments according to a geometrical series in order to tighten the time steps toward the end of t_F. This was necessary to avoid numerical problems. For broken elements and matrix elements, the constants of state must also be updated and the aforementioned process repeated until failure occurs.

Failure Criteria

The composite is considered as having failed if one of two failure criteria is satisfied. The most obvious failure mode is the formation of a cleavage plane; i.e., all of the fiber elements situated in one plane across the elements are broken. The composite is considered as having failed since it has been assumed that only the fibers can carry tensile stress. The second failure mode is due to the lack of equilibrium of the composite under stress. Numerically, this corresponds to the occurrence of a singular stiffness matrix. For example, this failure mode occurs when two cleavage planes are joined by matrix failure.

Input Data

The model described herein was applied to a simplified example consisting of 15 fibers each discretized into 15 finite-difference elements. The input data used for the example is shown in Table 2. The distance between two neighboring fibers is deduced by taking the thickness of the monolayer as being equal to the fiber diameter and by considering the percentage of fibers by volume. The elastic constant of the fiber (elastic modulus) corresponds to E-glass while that of the matrix (shear modulus) corresponds to an epoxy.

Results and Discussion

As before two environments were considered: water and acid. Two probability distributions for flaw size were considered for illustration. Both of them are normal with a mean of 2.5° and a variance of 0.5° for the first and a mean of 1.7° and a variance of 0.3° for the second. For each simulation run, the flaws in each fiber element were selected randomly by sampling from the adopted flaw size distribution. The applied stress was increased in

J. Compos. Constr. 2003.7:109-117.

Table 2. Input Data Used in Present Simulation

Data criteria	Value
Percentage of fibers by volume (%)	50.0
Radius of fiber (μm)	6.5
Distances between fibers (μm)	7.81
Thickness of monolayer (μm)	13.0
Fiber element length (μm)	130.0
Fiber elastic modulus (GPa)	70.0
Shear strength of matrix (MPa)	39.0
Shear yield stress of matrix (MPa)	18.5
Matrix shear modulus (GPa)	1.327
Work hardening coefficient of matrix	0.01

increments of 0.1 GPa for the first distribution and in increments of 0.3 GPa for the second one. 50 runs or simulations were carried out for each stress level.

Fig. 8 shows the simulations obtained with both flaw size distributions. It shows also experimental results compiled by Phoenix (2000). The experimental results, presented here as the 0% and 100% time-to-failure quartiles, were obtained for S-glass/epoxy strands tested in stress rupture at Lawrence Livermore National Laboratory in the 1970's (Chiao et al. 1972). It can be seen that the simulation with a flaw distribution having a mean of 1.7° lies exactly on the 0% time-to-failure quartile. This is a very encouraging result since the experimental results were obtained for S-glass, which is known to be more corrosion resistant than E-glass. The ultimate strength predicted by simulation is about 3.3 GPa. This is about correct when compared to the known strength of E-glass unidirectional composite, which lies between 2.5 and 3.5 GPa.

The simulation results with the flaw size probability distribution having a mean of 2.5 are well below the 0% time-to-failure quartile. The ultimate strength predicted with this distribution is about 1.2 GPa, which is much less than the known strength of E-glass unidirectional composite. Given the length of the fiber element considered, this observation supports the earlier conclusion that flaw of A, which has less probability of occurrence over the same gauge length than flaw B, corresponds indeed to flaw σ_1 with a depth of 0.01 μm.

Fig. 9 represents the results of the simulations for acid. As in the case of individual fibers (see Fig. 5), there is no experimental evidence to suggest which value of θ_0 leads to a better estimate of lifetime, except that the ultimate strength is best predicted with a half angle $\theta = 1.7°$. Again, it can be seen that stress corrosion in acid proceeds at a much faster rate, but this time for the composite material.

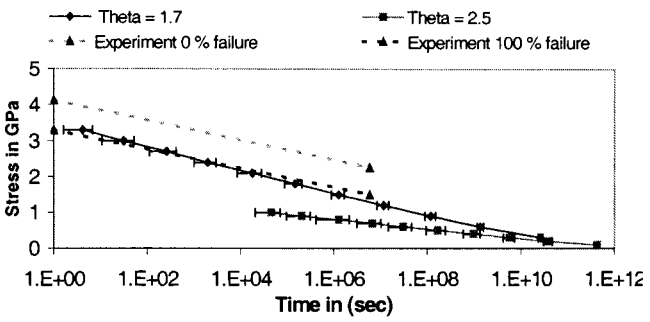

Fig. 8. Simulated stress corrosion life of E-glass unidirectional composite in water

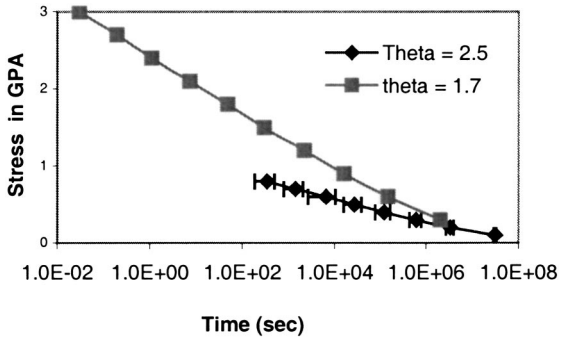

Fig. 9. Simulated stress corrosion life of E-glass unidirectional composite in acid

The simulation runs were dissected to extract the rupture patterns in the monolayer as a function of applied stress. This is shown in Figs. 10 and 11. Figs. 10 and 11 show the chronological order in which the fibers fail.The numbers at the right-hand side indicate the chronological order in which the fibers fail. At low stress (Fig. 10), the monolayer fails through the formation of a cleavage plane characteristic of stress corrosion failure (compare with Fig. 1). Fig. 11 shows a failure pattern reminiscent of testing to failure under monotonic loading. Fiber breakage occurs randomly over the monolayer, and monolayer failure occurs when two or more cleavage planes are joined by matrix failure. Numerically, this translates into a pivot being equal to zero in the system stiffness matrix.

Figs. 12 and 13 are plane schematic representations of the cylindrical monolayer. In both figures, an incubation period is evident. At low stress (Fig. 12), about one third of the fibers fail sequentially. This lasts for about 99% of the life of the composite. Then, the composite fails suddenly in a brief succession of fiber breaks. This was experimentally observed by Swit (2000). At high stresses (Fig. 13), the incubation period covers less that a third of fiber breaks, and failure of the composite is more sudden.

Conclusion

We have proposed a methodology for life prediction of unidirectional GFRP in tension. The model is based both on a well-established knowledge on the chemical behavior of glass and, in particular, that of glass flaws and more recent models of stress corrosion. These were combined with fracture mechanics, a shear lag model, simulation and a probability model for flaw size to

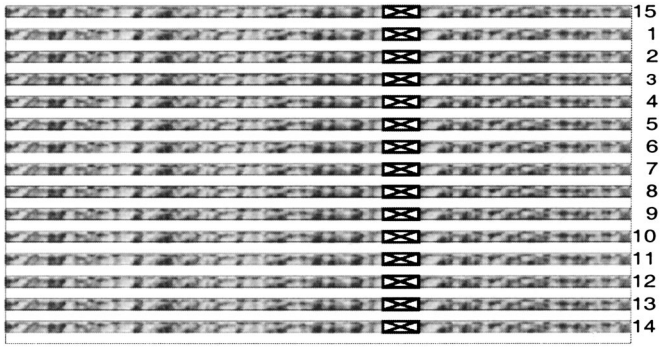

Fig. 10. Failure pattern at low stress (0.3 GPa) in water

J. Compos. Constr. 2003.7:109-117.

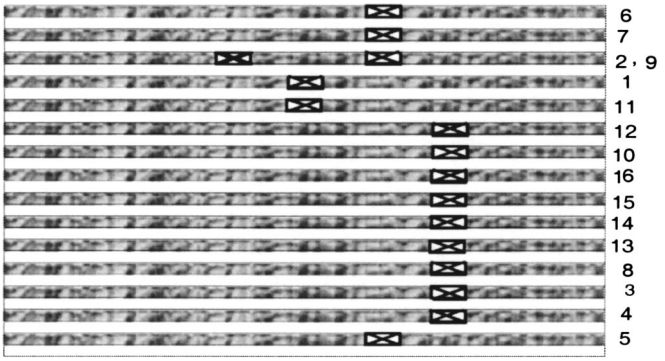

Fig. 11. Failure pattern at high stresses (2.7 GPa) in water

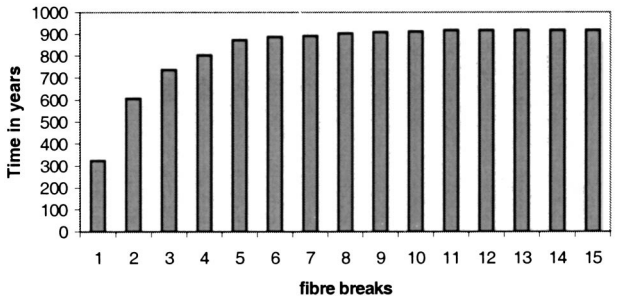

Fig. 12. Chronological of fiber breaks in water at .3 GPa

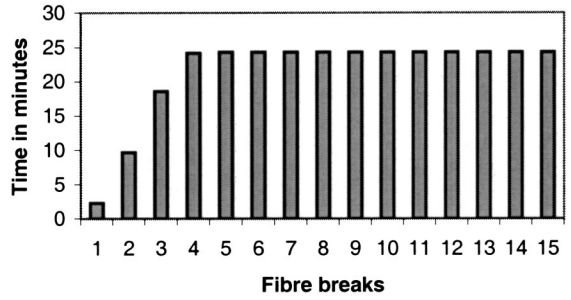

Fig. 13. Chronological of fiber breaks in water at 2.7 GPa

develop a model for the description of the behavior of GFRP composite subject to stress corrosion.

The model suggests that the flaws responsible for stress corrosion are mild surface flaws that are approximately 10^{-2} cm apart. When they are assumed to be circular in shape, the model suggests, by comparison to limited experimental data, that the flaws have a half angle θ of approximately 1.7°, which corresponds to a depth of 0.009 μm.

The stress corrosion cracking of GFRP was found to have an incubation period in which about a third of the fiber break. Thereafter, the stress concentration reaches such a high level that unstable crack growth occurs. This corroborates the generally recognized catastrophic failure of static fatigue (Swit 2000). At low stress levels, the fracture pattern is that of stress corrosion as obtained experimentally; a cleavage plane runs perpendicular to the longitudinal direction of the fibers. At high stresses, the failure pattern simulated corresponds to that of ultimate strength testing under monotonic loads in which matrix failure under shear plays a major role.

The results of the present study, although limited to a rather idealized situation, are very encouraging. They suggest that, with only modest assumptions about material properties, it is possible to obtain mechanisms of GFRP breakdown, which corresponds to experimental behavior, at least for the known test results. The model also permits an estimation of the time to failure under different environmental conditions. As far as can be ascertained, this has not previously been done and reported in literature.

Acknowledgment

This study forms part of a research program funded by the Cooperative Research Center for Advanced Composite Structures (CRC-ACS, Ltd.) Australia.

Notation

The following symbols are used in this paper:

A = cross-sectional area of fiber;
a = crack length;
$C_{1(i,j)}$, $C_{2(i,j)}$, $C_{3(i,j)}$, $C_{4(i,j)}$, $C_{5(i,j)}$ = constants of linear system of equations;
$C_{(i,j)}$ = constants forming right-hand side of linear system of equations;
C_E = concentration of acid;
d_i = distance between ith and the $(i+1)$th fiber;
E = Young's modulus of fiber;
E_a = activation energy of reaction of glass to water;
$F(i,j)$ = fiber element;
G = elastic shear modulus of matrix;
h = thickness of monolayer;
K_I = stress intensity factor for opening model I;
K_{so} = reaction rate constant of glass to acid;
$M(i,j)$ = matrix element;
N = number of fibers in monolayer;
n = molar ratio of glass to acid;
R = universal gas constant;
r = radius of glass fiber;
T = absolute temperature;
t_F = lifetime of glass fiber subject to stress corrosion;
α = empirical constant;
$\alpha_{i,j}$ = Heaviside's step functions relative to state of fiber element;
$\beta_{i,j}$, $\beta_{i,j}$ = functions relative to state of matrix element;
Δt = time duration between two successive fiber breaks;
Δx = length of fiber element;
ν = empirical constant;
σ = stress acting on glass fiber;
σ_{ap} = stress applied to monolayer;
σ_i = normal stress working along ith fiber;
τ_i = shear stress in the matrix between ith and $(i+1)$th fiber;
τ_{max} = matrix shear strength;
τ_y = shear yield stress of matrix;
θ = half angle of a flaw in glass fiber;
θ_0 = initial half angle of flaw in glass fiber; and
θ_F = final half angle of flaw in glass fiber.

References

Aveston, J., and Sillwood, J. M. (1982). "Long-term strength of glass reinforced plastics in dilute sulphuric acid." *J. Mater. Sci.*, 17, 3491–3498.

J. Compos. Constr. 2003.7:109-117.

Bartenev, G. M. (1969). ''Constitution and strength of glass fibers.'' *Int. J. Fract. Mech.*, 5, 179–186.
Charles, R. J. (1958a). ''Static fatigue of glass. I.'' *J. Appl. Phys.*, 29(11), 1549–1553.
Charles, R. J. (1958b). ''Static fatigue of glass. II.'' *J. Appl. Phys.*, 29(11), 1554–1560.
Chiao, T. T., Lepper, J. K., Hetherington, N. W., and Moore, R. L. (1972). ''Stress rupture of simple S-glass/epoxy composites.'' *J. Compos. Mater.*, 6, 358–370.
Goda, K., and Fukunaga, H. (1989). ''Considerations of the reliability of tensile strength at elevated temperature of unidirectional metal matrix composites.'' *Compos. Sci. Technol.*, 35, 181–193.
Goda, K., and Phoenix, S. L. (1994). ''Reliability approach to the tensile strength of unidirectional CFRP composites by Monte Carlo simulation in a shear lag model.'' *Compos. Sci. Technol.*, 457–468.
Guild, F. J., Vlattas, C., and Galiotis, C. (1994). ''Modeling of stress transfer in fiber composites.'' *Compos. Sci. Technol.*, 50, 319–332.
Hedgepeth, J. M., Dyke, Van (1967). ''Local stress concentrations in imperfect filamentary composite materials.'' *J. Compos. Mater.*, 1, 294–309.
Hogg, P. J., and Hull, D. (1982). ''Micromechanics of crack growth in composite materials under corrosive environments.'' *Met. Sci.*, 17, 441–450.
Hsu, P. L., Yau, S. S., and Chou, T. W. (1986). ''Stress corrosion cracking and its propagation in aligned short fiber composites.'' *J. Mater. Sci.*, 21, 3703–3709.
Lhymn, C., and Schultz, J. M. (1983). ''Chemically assisted fracture of thermoplastic PET reinforced with short E-glass fiber.'' *J. Mater. Sci.*, 18, 2923–2938.
Loewenstein, K. L. (1973). *The manufacturing technology of continuous glass fibers*, Elsevier, London.
Lyons, K. B., and Phillips, M. G. (1981). ''Creep rupture and damage mechanisms in glass reinforced plastics.'' *Composites*, 12(4), 265–271.
McBagonluri, F. (1998). ''Simulation of fatigue performance and creep rupture of glass-reinforced polymeric composites for infrastructure applications.'' MS thesis, Virginia Polytechnic Institute and State University, Va.
Mould, R. E. (1960). ''Strength and static fatigue of abraded glass under controlled ambient conditions. III, Aging of fresh abrasions.'' *J. Am. Ceram. Soc.*, 43, 160–167.
Oh, K. P. (1979). ''A Monte Carlo study of the strength of unidirectional fiber-reinforced composites.'' *J. Compos. Mater.*, 13, 311–328.
Phillips, M. G. (1983). ''Prediction of long term stress-rupture life for glass fiber reinforced polyester composites in air and aqueous environments.'' *Composites*, 14(3), 270–275.
Phoenix, S. L. (2000). ''Modeling the statistical lifetime of glass fiber/polymer matrix composites in tension.'' *Compos. Struct.*, 48, 19–29.
Price, J. N., and Hull, D. (1987). ''Effect of matrix toughness on crack propagation during stress corrosion of glass reinforced composites.'' *Compos. Sci. Technol.*, 28, 193–210.
Reedy, Jr., E. D. (1984). ''Fiber stresses in a cracked monolayer: Comparison of shear lag and 3D finite-element predictions.'' *J. Compos. Mater.*, 18, 595–607.
Roberts, R. C. (1978). ''Design strain and failure mechanisms of GRP in a chemical environment.'' *Proc., Reinforced Plastics Congress*, British Plastics Federation, 145–151.
Sastry, A. M., and Phoenix, S. L. (1993). ''Load redistribution near non-aligned fiber breaks in a two-dimensional unidirectional composite using break-influence superposition.'' *J. Mater. Sci. Lett.*, 12, 1596–1599.
Schmitz, G. K., and Metcalfe, A. G. (1965). ''Characterization of flaws on glass fibers.'' *Proc., 20th Anniversary Technical Conf.*, The Society of the Plastics Industry, Inc., 1–14.
Schmitz, G. K., and Metcalfe, A. G. (1966). ''Stress corrosion of E-glass fibers.'' *I&EC Products Res. Dev. Indust. Eng. Chem.*, 5(1), 1–8.
Schutte, C. L. (1994). ''Environmental durability of glass-fiber composites.'' *Mater. Sci. Eng., R.*, 13(7), 265–324.
Sekine, H. (1991). ''Micromechanics study of the propagation rate of a stress corrosion crack in cross ply glass/epoxy laminates under acid environments.'' *Proc., 8th Int. Conf. on Composite Materials*, SAMPE, Covina, Ca., 27-k-1–27-k-10.
Sekine, H., Hu, N., and Fukunaga, H. (1995). ''Direct numerical simulation of the extension of stress-corrosion cracks in glass fibers embedded in laminates in acid environments.'' *Compos. Sci. Technol.*, 53, 317–323.
Sekine, H., and Beaumont, P. W. R. (1998). ''A physically based micromechanical theory and diagrams of macroscopic stress-corrosion cracking in aligned continuous glass-fiber-reinforced polymer laminates.'' *Compos. Sci. Technol.*, 58, 1659–1665.
Swit, G. (2000). ''Durability of stressed E-glass fibre in alkaline medium.'' In *Recent developments in durability analysis of composite systems*, Cardon, Fukuda, Reifsneider, and Verchery, eds., Balkema, Rotterdam, The Netherlands, 473–476.
Wiederhorn, S. M., and Bolz, L. H. (1970). ''Stress corrosion and static fatigue of glass.'' *J. Am. Ceram. Soc.*, 53(10), 543–548.
Zhou, S. J., and Curtin, W. A. (1995). ''Failure of fiber composites: A lattice Green function model.'' *Acta Metall. Mater.*, 43(8), 3093–3104.

J. Compos. Constr. 2003.7:109-117.